Self-Assembly of Au@Ag Nanorods Mediated by Gemini Surfactants for Highly Efficient SERS-Active Supercrystals

Sergio Gómez-Graña, Jorge Pérez-Juste, Ramón A. Alvarez-Puebla, Andrés Guerrero-Martínez, and Luis M. Liz-Marzán**

Research on efficient substrates for surface-enhanced Raman scattering (SERS) spectroscopy has recently focused on 3D plasmonic supercrystals,[1] with the aim of obtaining crystalline superlattices of metal nanoparticles with intense and controlled antenna effects, which result in huge electric field concentration.[2] The self-assembly of colloidal metal nanoparticles based on the interactions between molecules located at the nanocrystal surfaces has proven the most effective approach toward controlling nanoparticle spacing in 3D substrates.[3] In this context, anisotropic plasmonic nanoparticles such as gold nanorods (AuNRs) have been used to prepare SERS supercrystal substrates with uniform and high plasmonic antenna enhancements of the electric field.[4] Notwithstanding, the efficiency of the fabrication of self-assembled supercrystals as optical sensors with the potential to maximize SERS signals can be improved by just replacing gold with silver and/or by refining substrate production.[5]

Aiming at the high self-assembly efficiency of biomolecules such as DNA or proteins, synthetic bio-inspired capping agents have gained popularity as surface templates in the formation of self-assembled colloidal supercrystals over micrometer length scales.[6] Among them, gemini surfactants comprising two hydrophobic tails and two hydrophilic headgroups linked by a molecular spacer,[7] have proven excellent stabilizers and binders in nanoparticle synthesis and self-assembly,[8] since they may mimic the bilayer formation of phospholipids in biomembranes.[9] In fact, we have recently investigated the structural role of gemini surfactants on the controlled synthesis of monodisperse AuNRs that self-assemble into ordered, standing 2D and 3D superlattices by simple drop casting.[10] Considering the higher plasmonic efficiency of silver nanoparticles,[11] and encouraged by the need of optimization of the self-assembly process that may allow the design of large-scale supercrystals with high optical activity for SERS detection, we report on a straightforward approach to obtain long-range plasmonic supercrystals made of standing core-shell gold-silver nanorods (Au@AgNRs), stabilized with gemini surfactants, by controlling the drop casting conditions.

Au@AgNRs (length = 71 ± 3 nm; width = 34 ± 2 nm) were prepared from single crystal AuNR seeds (length = 68 ± 4 nm; width = 13 ± 1 nm) following a synthetic protocol for the controlled reduction of silver ions onto AuNRs, adapted from the work by Vaia and co-workers (see Supporting Information).[12] The mixture of conventional surfactants originally employed during the growth was replaced by the gemini surfactant bis(dodecyldimethylammonium)diethyl ether bromide (16-EO1–16).[13] The success of the synthesis is exemplified in **Figure 1**, where the UV/vis absorbance spectra of the

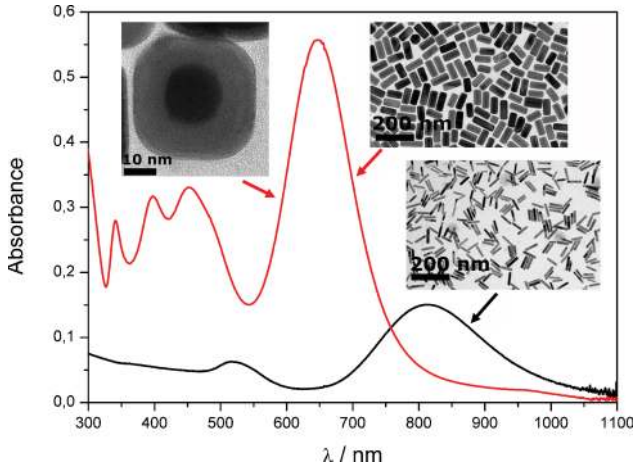

Figure 1. UV/vis absorbance spectra of the AuNR seeds (black) and the final Au@AgNRs (red) synthesized with 16-EO1-16 surfactant. The insets show representative TEM micrographs of the corresponding AuNRs and Au@AgNRs (upper left inset is the cross section of one Au@AgNR).

S. Gómez-Graña, Prof. J. Pérez-Juste,
Prof. L. M. Liz-Marzán
Departamento de Química Física
Universidade de Vigo
36310, Vigo, Spain
E-mail: llizmarzan@cicbiomagune.es
Prof. R. A. Alvarez-Puebla
ICREA (Catalan Institution for Research and Advanced Studies)
Passeig Lluis Companys 23, 08010 Barcelona, Spain
Prof. R. A. Alvarez-Puebla
Department of Electronic Engineering
Universitat Rovira i Virgili
Avda. Paisos Catalans 26, 43007 Tarragona, Spain
Prof. R. A. Alvarez-Puebla
Center for Chemical Technology of Catalonia
Edifici N5, Carrer de Marcellí Domingo s/n, 43007, Tarragona, Spain
Dr. A. Guerrero-Martínez
Departamento de Química Física I
Universidad Complutense
Avda. 20 Complutense s/n, 28040, Madrid, Spain
E-mail: aguerrero@quim.ucm.es
Prof. L. M. Liz-Marzán
BioNanoPlasmonics Laboratory
CIC biomaGUNE, Paseo de Miramón 182,
20009 Donostia - San Sebastián, Spain
Prof. L. M. Liz-Marzán
Ikerbasque, Basque Foundation for Science
48011, Bilbao, Spain

DOI: 10.1002/adom.201300162

AuNR seeds and the corresponding final Au@AgNR colloids in aqueous solution are displayed, together with representative transmission electron microscopy (TEM) images (see also the Supporting Information). Silver deposition led to an increase of the intensity and blue-shift of both the longitudinal and transverse localized surface-plasmon resonance (LSPR) bands of the AuNRs, at 815 and 520 nm, respectively (Figure 1), which is in agreement with previous reports on the effect of combining the plasmonic response of gold an d silver nanostructures.[11] Additionally, other high-energy modes arise upon reduction of silver onto the AuNRs. The optical properties of similar Au@Ag nanocuboids have been recently studied by several authors,[14,15] who provided a full description of their plasmonic responses. The spectrum of the Au@AgNRs consistently presents the LSPR bands associated with a longitudinal LSPR (647 nm), a transverse LSPR (453 nm), and two higher order hybrid modes (397 and 341 nm). TEM analysis shows that after silver coating, the nanorod aspect ratio decreases significantly from 5.2 to 2.1 (see Supporting Information), which reflects a favored growth of silver on high index lateral facets.[16,17] TEM clearly shows that the final Au@AgNRs present a core–shell morphology with an external rectangular prism morpholgy (Figure 1).

Optimization of the preparation of 3D supercrystals from Au@AgNRs was carried out by drop casting 10 µL volumes of the colloidal solution ([16-EO1–16] = 10^{-3} M, [Au@AgNRs] = 10^{-5} M) at controlled temperature (20, 30 and, 40 °C) and humidity (35, 60, and 90%) conditions on indium tin oxide (ITO)-covered glass substrates (see Supporting Information). A direct consequence of the interfacial aggregation properties of 16-EO1–16 at interfaces can be gathered from the scanning electron microscopy (SEM) images shown in **Figure 2**. Spontaneous formation of self-assembled superlattices of Au@AgNRs was readily observed at optimized drop casting conditions (20 °C and 90% humidity). In good agreement with previous studies of AuNRs stabilized with gemini surfactants,[10] the deposition of nanoparticles typically resulted in the formation of coffee ring deposits (~40–70 µm wide and ~5 mm external diameter, Figure 2a,b) and a significant amount of inner coffee ring deposits.[18] As shown in Figure 2b, three different adjacent and concentric ring regions were observed at the coffee ring pattern. Whereas disordered nanoparticle assemblies formed at the outer edge (1) (Figure 2c), with ring widths smaller than 10 µm, Au@AgNRs self-assembled into standing supercrystals in the intermediate ring region (2) (Figure 2d), where layers of nanocrystals span ~40 µm across with an extraordinary long-range order. Figure 2e also shows a representative micrograph of the inner edge (3) of the coffee ring deposit (ring widths < 15 µm), in which a multilayer 3D array of lying Au@AgNRs can be observed. From a closer view of Figure 2d and e, it can be stated that Au@AgNRs self-assemble with a simple tetragonal arrangement ($a = b = 38$ nm, $c = 75$ nm) and an interparticle distance of 3.5 ± 1 nm (see the fast Fourier transform of the SEM micrograph in Figure 2d in the Supporting Information),[19] in which each bilayer of side-by-side nanorods is ordered without shifts with respect to the adjacent layers in the *c* direction of the arrangement. This result differs from the typical hexagonal close-packed arrangement obtained in the case of AuNRs,[20] in which each nanorod monolayer is shifted by half the interparticle distance with respect to the adjacent layers.[10] We attribute this difference to the rectangular prism structure of the core-shell particles,[12,14] in which the characteristic curvature of AuNRs[17] is lost during silver deposition.

The dimensions of the ordered region (2) formed by standing Au@AgNR supercrystals within the nanoparticle ring deposits are summarized in **Table 1**. In contrast to the non-significant changes observed at low relative humidities (35 and 60%), long-range extensions of the 3D standing supercrystals are obtained at high relative humidity (90%). Additionally, the width of region (2) decreases when increasing deposition temperature form 20 to 40 °C, indicating that slow water evaporation is beneficial for the extension of the supercrystal (see Supporting Information). These results are in good agreement with the formation of an intermediate smectic-B liquid-crystalline phase of nanoparticles upon controlled and slow solvent evaporation.[21,22] **Figure 3** illustrates the UV/Vis/NIR absorbance spectra of the Au@AgNRs colloidal solution together with the nanoparticle coffee ring deposits obtained by drop casting onto ITO-covered glass substrates at 20 °C and relative humidities of 90% and 35%. As expected, broadening and red shift of all plasmon modes occur,

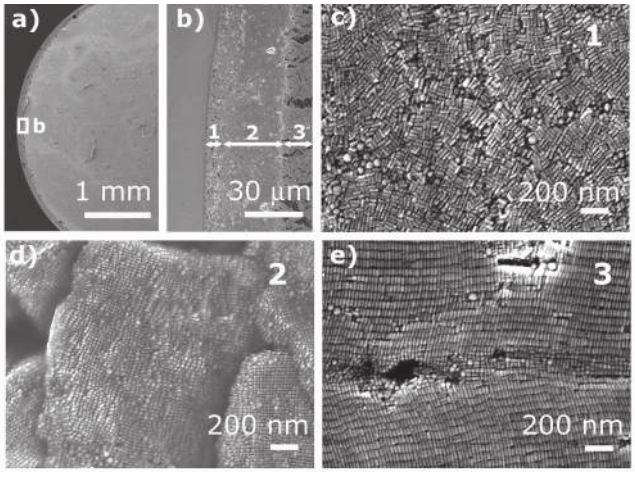

Figure 2. SEM micrographs of Au@AgNRs on ITO-coated glass slides, deposited at optimized drop casting conditions ([16-EO_1-16] = 10^{-3} M, [Au@AgNR] = 10^{-5} M, relative humidity = 90% and T = 20 °C). (a) Partial view of the drop pattern formed upon casting. (b) Magnification of the coffee ring deposits in (a), where three concentric ring regions are observed. (c) Enlarged view of region (1) showing disordered assembled Au@AgNRs (ring width < 10 µm). (d) Partial view of region (2) that shows the existence of standing 3D supercrystals (ring width ~ 40 µm). (e) Region (3) in which 3D supercrystals of lying NRs are observed (ring widths < 15 µm).

Table 1. Average widths (±2 µm) of the supercrystal intermediate layer (2) of Au@AgNRs drop casted on ITO at different environmental conditions (temperature and relative humidity).

Temperature [°C]	Relative Humidity (%)		
	35	60	90
20	14 µm	17 µm	40 µm
30	15 µm	16 µm	30 µm
40	12 µm	15 µm	25 µm

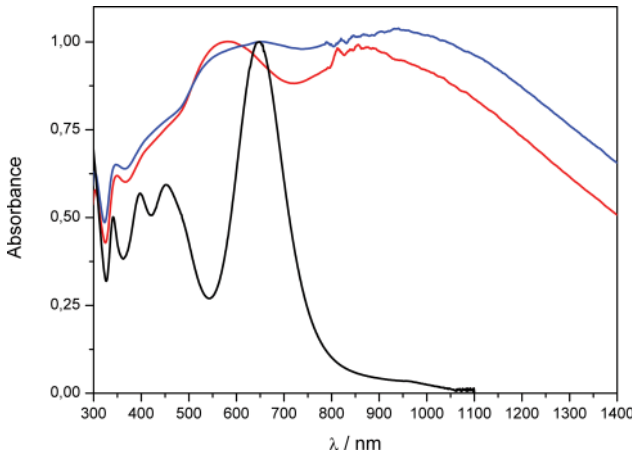

Figure 3. Normalized UV/vis/NIR absorbance spectra of the Au@AgNRs colloid solution (black) and the corresponding coffee ring deposits obtained by drop casting at 20 °C, and relative humidities of 90% (red) and 35% (blue) onto ITO-coated glass substrates.

as a consequence of plasmon coupling between the close-packed Au@AgNRs at the coffee ring deposits.[21] The spectrum of the Au@AgNR deposits upon excitation by non-polarized UV/vis/NIR irradiation perpendicularly oriented to the substrates, displays a less intense lower energy mode (~900 nm), whereas the transverse LSPR (~582 nm) and the two high energy hybrid modes (~420 and 348 nm) increase in intensity, as compared to the spectrum in solution. Therefore, the observed collective LSPR responses indicate that Au@AgNRs are preferentially assembled within standing supercrystals at the coffee ring deposits, especially in the case of 90% humidity, where a higher intensity of the transverse LSPR is observed (Figure 3), in good agreement with the spanning dimensions obtained for region (2) at different humidities (Table 1).

Characterization of the SERS enhancing efficiency of the Au@AgNR supercrystals was carried out using benzenethiol (BT), a well-known SERS probe. BT was retained on the supercrystals surface from the gas phase. For the sake of comparison, another colloidal crystal was prepared at the same optimized concentrations and drop casting conditions, with the AuNRs used as seeds during the silver overgrowth process (**Figure 4**). After controlled drying, hexagonal close-packed arrangements of AuNRs with an average interparticle distance of 3.0 ± 1 nm were obtained (see the fast Fourier transform of the SEM micrograph in Figure 4b in the Supporting Information). Although thiol groups have a high affinity for both silver and gold, the stability constant is considerably higher for gold (pK = 25) than for silver (pK = 12).[23] However, due to the similar crystallographic structure of both metals, similar size of the constituent nanoparticle building blocks and retention method from the gas phase (up to total surface coverage), we can assume a similar number of molecules on both surfaces. Direct comparison is thus possible. Although the characteristic SERS spectrum of BT was clearly identified in both supercrystals, those composed by Au@AgNRs yielded 4 fold more intensity (**Figure 5**). This is consistent with the fact that silver is a much more efficient optical enhancer, and for similar particle size and shape, it yields enhancement factors (EFs) 2 or 3

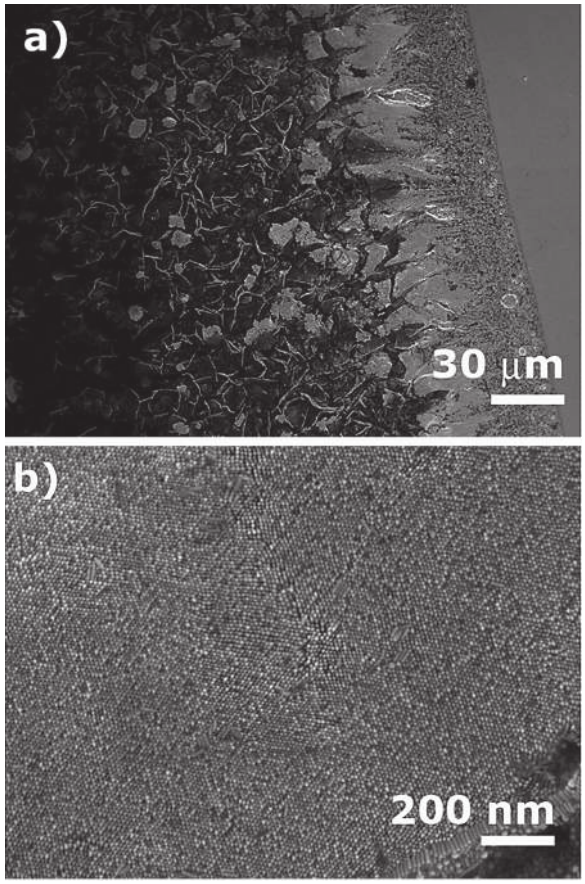

Figure 4. SEM micrographs of AuNRs on ITO, obtained at optimized drop casting conditions ([16-EO1-16] = 10^{-3} M, [AuNR] = 10^{-5} M, relative humidity = 90% and T = 20 °C). (a) Magnification of the coffee ring deposits. (b) Enlarged view of region (2) showing standing 3D supercrystals (ring width ~ 30 µm).

orders of magnitude larger than those of gold.[11] In our case, silver is a small coating on gold nanorods and accordingly, the extra enhancement is smaller than that expected for pure silver rods.[11] To test for the homogeneity of the signal intensity, a key parameter for the development of quantitative applications, SERS mapping was carried out over an extended area (30 × 135 µm, step size 1 µm). Notably three different regions, (1) to (3) in Figure 5a, are observed, in good agreement with the SEM and UV/Vis/NIR results (Figure 2 and 3). Region (1) is characterized by the formation of conventional but randomly distributed tip to tip and/or side to side hotspots,[24] while regions (2) and (3) show supercrystals either standing or lying, respectively. When comparing the SERS intensities it becomes clear that randomly distributed nanorods cannot compete with the highly organized superstructures (Figure 5c). Standing supercrystals offer EF about two orders of magnitude larger than that of the random hot spot system. In the case of the lying crystals, the EF is about 20 fold larger. This last observation also indicates the importance of the geometric orientation of the anisotropic constituents in the supercrystal. Although both are ordered 3D structures, the standing crystals give rise to 4 fold more intensity than the lying structures. This

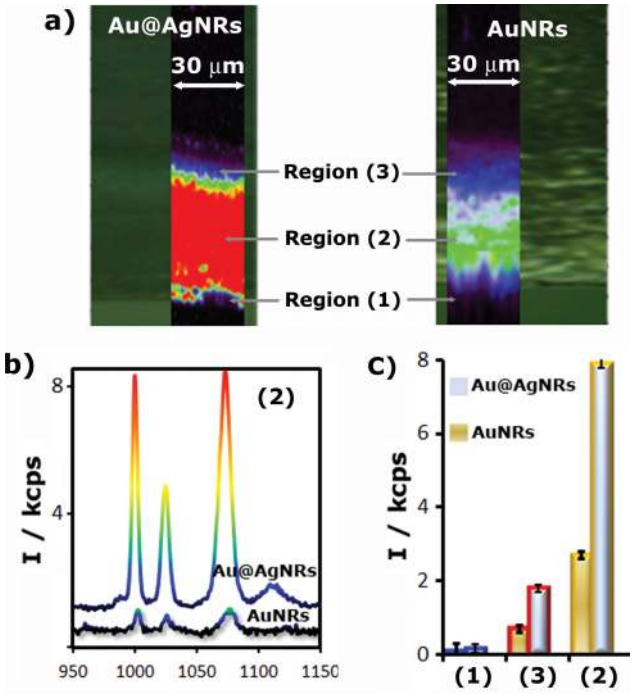

Figure 5. (a) Drop profile and SERS mapping of BT (1072 cm^{-1}, ring breathing) evaporated on Au@AgNRs and AuNRs coffee ring deposits (optimized drop casting conditions on ITO: 20 °C and 90% humidity). Excitation laser line = 633 nm, power at the sample 1mW, acquisition time 200 ms, 30 × 135 μm, step size 1 $μm^2$ and 4050 spectra. (b) SERS spectra of BT on region (2) of Au@AgNRs and AuNRs supercrystals. (c) Comparisons between BT SERS intensities (1072 cm^{-1}) on Au@AgNRs and AuNRs supercrystals at the different ring regions (1), (2) and (3).

observation cannot be simply explained in light of the formation of a dense and ordered collection of hot spots but as the electric field transfer on the supercrystal.[4]

In conclusion, the optimization of the self-assembly of Au@AgNRs in standing supercrystals at the coffee ring deposits under drop casting has been used to fabricate SERS substrates with long-range sensing areas (2–3 × $10^5 μm^2$), uniform electric field enhancement and high intensity hot spots. Au@AgNRs SERS-active supercrystals have been demonstrated to overperform their AuNRs counterparts as SERS substrates. We thus anticipate the use of these novel highly optically active sensors as a new type of SERS substrates that offer new possibilities for ultrasensitive screening of analytical targets relevant to medical and environmental science.

Experimental Section

Synthesis of the Gemini Surfactant: The gemini surfactant bis(dodecyl dimethylammonium)diethyl ether bromide (16-EO1–16) (see Supporting Information), was synthesized according to procedures previously described in the literature.[13]

Synthesis of Gold Nanorods (AuNRs): AuNRs were prepared by the seeded growth method.[25] The seed solution was made mixing a CTAB solution (4.7 mL, 0.1 M) with 25 μL of 0.05 M $HAuCl_4$; this solution was kept at 30 °C for 5 min and afterwards 300 μL of sodium borohydride 0.01 M was added quickly under vigorous stirring. The resulting solution was kept at 30 °C. An aliquot of seed solution (24 μL) was added to a growth solution (10 mL) containing CTAB (0.1 M), $HAuCl_4$ (0.5 mM), ascorbic acid (0.8 mM), $AgNO_3$ (0.12 mM), and HCl (18.6 mM). The reaction beaker was kept at 30 °C overnight. AuNRs were washed by centrifugation twice (8000 rpm, 25 min), the supernatant was discarded and the precipitate was redispersed in 10 mL of gemini surfactant 16-EO1–16 50 mM solution. Four hundred particles were measured on TEM images to determine the aspect ratio (5.2 ± 0.5), and the average length (68 ± 4 nm) and width (13 ± 1 nm) of the AuNRs (Figure S2). The errors of aspect ratio and dimensions represent standard deviations.

Silver Overgrowth on Gold Nanorods (Au@AgNRs): Silver coating was made following a modification of a procedure previously reported by Vaia et al.[12] A growth solution (5 mL) was prepared by mixing under stirring 5 mM of 16-EO1–16, 1 mM of $AgNO_3$, 0.25 mM of Au^0 as seed AuNRs, and 4 mM of ascorbic acid. After the last addition, the temperature was raised to 60–65 °C and maintained for 3 h. The solution was then centrifuged (6000 rpm, 20 min) and redispersed in water. Four hundred Au@AgNRs particles were measured on TEM images to determine the aspect ratio (2.1 ± 0.3), and the average length (71 ± 3 nm) and width (34 ± 2 nm) of the Au@AgNRs (Figure S2). The errors of aspect ratio and dimensions represent standard deviations.

Characterization of Nanorods: Transmission electron microscopy (TEM) images were obtained with a JEOL JEM 1010 transmission electron microscope operating at an acceleration voltage of 100 kV. Optical characterization was carried out by UV/vis/NIR spectroscopy with a Cary 5000 spectrophotometer using 10 mm path length quartz cuvettes for aqueous NR solutions.

Supercrystal Preparation: The preparation of supercrystals of Au@AgNRs and AuNRs in coffee ring deposits were carried on ITO-coated glass slides using the previously described colloidal solutions of monodisperse nanorods in water. To control the extent of the self-assembly, previously optimized conditions such as the concentration of 16-EO1–16 above the critical micelle concentration (1.0 mM), and the nanoparticle concentration (10^5 M) were kept constant.[10] Droplets (10 μL) were evaporated under controlled humidity (35, 60, and 90%) and temperature conditions (20, 30, and 40 °C) at a Envirotronics LH4003 Laboratory Test Chamber, taking the drying stage after several hours.

Supercrystals Characterization: Scanning electron microscopy (SEM) images of Au@AgNRs and AuNRs supercrystals have been obtained using a JEOL JSM-6700F FEG scanning electron microscope operating at an acceleration voltage of 5.0 kV for secondary-electron imaging (SEI). Optical characterization was carried out by UV/vis/NIR spectroscopy with a Cary 5000 spectrophotometer using 1 mm thick ITO-coated glass slides for NR assemblies.

Characterization of SERS Enhancement Efficiency: In order to characterize the Au@AgNRs and AuNRs supercrystals films, benzenethiol (BT) was adsorbed from the gas phase over the whole surface of the films by casting a drop of BT (0.1 M in ethanol) on a Petri dish where the film was also contained. Surfaces were then mapped in a Renishaw Invia System using the Renishaw StreamLine accessory with a 50× objective. Mapping areas of 30 × 135 $μm^2$, with a step size of 1 μm (40 × 40 spectra each) were recorded upon excitation with a 633 nm (HeNe) laser line. Acquisition times were set to 200 ms with power at the sample of 1 mW.

Supporting Information

Supporting Information is available from the Wiley Online Library or from the author.

Acknowledgements

This work has been funded by the European Research Council (ERC Advanced Grant #267867 Plasmaquo). A.G.-M. acknowledges receipt

of a Ramón y Cajal Fellowship from the Ministerio de Economía y Competitivdad.

Received: April 9, 2013
Revised: April 26, 2013
Published online: May 22, 2013

[1] H. Ko, S. Singamaneni, V. V. Tsukruk, *Small* **2008**, *4*, 1576.
[2] G. W. Bryant, F. J. García de Abajo, J. Aizpurua, *Nano Lett.* **2008**, *8*, 631.
[3] M. R. Jones, R. J. Macfarlane, B. Lee, J. Zhang, K. L. Young, A. J. Senesi, C. A. Mirkin, *Nat. Mater.* **2010**, *9*, 913.
[4] R. A. Alvarez-Puebla, A. Agarwal, P. Manna, B. P. Khanal, P. Aldeanueva-Potel, E. Carbó-Argibay, N. Pazos-Pérez, L. Vigderman, E. R. Zubarev, N. A. Kotov, L. M. Liz-Marzán, *Proc. Natl. Acad. Sci. USA* **2011**, *108*, 8157.
[5] A. Guerrero-Martínez, M. Grzelczak, L. M. Liz-Marzán, *ACS Nano* **2012**, *6*, 3655.
[6] W. Cheng, M. J. Campolongo, J. J. Cha, S. J. Tan, C. C. Umbach, D. A. Muller, D. Luo, *Nat. Mater.* **2009**, *8*, 519.
[7] a) F. M. Menger, J. S. Keiper, *Angew. Chem.* **2000**, *112*, 1980; b) F. M. Menger, J. S. Keiper, *Angew. Chem. Int. Ed.* **2000**, *39*, 1906.
[8] M. S. Bakshi, *Langmuir* **2009**, *25*, 12697.
[9] M. Muñoz-Úbeda, S. K. Misra, A. L. Barrán-Berdón, C. Aicart- Ramos, M. B. Sierra, J. Biswas, P. Kondaiah, E. Junquera, S. Bhattacharya, E. Aicart, *J. Am. Chem. Soc.* **2011**, *133*, 18014.
[10] A. Guerrero-Martínez, J. Pérez-Juste, E. Carbó-Argibay, G. Tardajos, L. M. Liz-Marzán, *Angew. Chem. Int. Ed.* **2009**, *48*, 9484.
[11] M. F. Cardinal, B. Rodríguez-González, R. A. Alvarez-Puebla, J. Pérez-Juste, L. M. Liz-Marzán, *J. Phys. Chem. C* **2010**, *114*, 10417.
[12] K. Park, L. F. Drummy, R. A. Vaia, *J. Mater. Chem.* **2011**, *21*, 15608.
[13] G. Tardajos, T. Montor, M. H. Viñas, M. A. Palafox, A. Guerrero-Martínez, *J. Phys. Chem. B* **2008**, *112*, 15691.
[14] M. B. Cortie, F. Liu, M. D. Arnold, Y. Niidome, *Langmuir* **2012**, *28*, 9103.
[15] R. Jiang, H. Chen, L. Shao, Q. Li, J. Wang, *Adv. Mater.* **2012**, *24*, OP200.
[16] Y. Yang, W. Wang, X. Li, W. Chen, N. Fan, C. Zou, X. Chen, X. Xu, L. Zhang, S. Huang, *Chem. Mater.* **2013**, *25*, 34.
[17] B. Goris, S. Bals, W. Van den Broek, E. Carbó-Argibay, S. Gómez- Graña, L. M. Liz-Marzán, G. Van Tendeloo, *Nature Mater.* **2012**, *11*, 930.
[18] T. A. H. Nguyen, M. A. Hampton, A. V. Nguyen, *J. Phys. Chem. C* **2013**, *117*, 4707.
[19] S. Gómez-Graña, F. Hubert, F. Testard, A. Guerrero-Martínez, I. Grillo, L. M. Liz-Marzán, O. Spalla, *Langmuir* **2012**, *28*, 1453.
[20] Y. Xie, Y. Jia, Y. Liang, S. Guo, Y. Ji, X. Wu, Z. Chen, Q. Liu, *Chem. Commun.* **2012**, *48*, 2128.
[21] C. Hamon, M. Postic, E. Mazari, T. Bizien, C. Dupuis, P. Even-Hernandez, A. Jimenez, L. Courbin, C. Gosse, F. Artzner, V. Marchi-Artzner, *ACS Nano* **2012**, *6*, 4137.
[22] T. Ming, X. Kou, H. Chen, T. Wang, H.-L. Tam, K.-W. Cheah, J.-Y. Chen, J. Wang, *Angew. Chem.* **2008**, *120*, 9831; *Angew. Chem. Int. Ed.* **2008**, *47*, 9685.
[23] R. M. Smith, A. E. Martell, in: *Critical Stability Constants. Vol. 4: Inorganic complexes*, Plenum Press, New York, USA **1976**.
[24] J. Jiang, K. Bosnick, M. Maillard, L. Brus, *J. Phys. Chem. B* **2003**, *107*, 9964.
[25] B. Nikoobakht, M. A. El-Sayed, *Chem. Mater.* **2003**, *15*, 1957.